Blue-edge slow photons promoting visible-light hydrogen production on gradient ternary 3DOM

Blue-edge Slow Photons Promoting Visible-light Hydrogen Production on Gradient Ternary 3DOM TiO_2-Au-CdS Photonic Crystals

Heng Zhao[a], Zhiyi Hu[a,b], Jing Liu[a], Yu Li[a*], Min Wu[a*], Gustaaf Van Tendeloo[b,c], Bao-Lian Su[a,d,e*]

[a] State Key Laboratory of Advanced Technology for Materials Synthesis and Processing, Wuhan University of Technology, 122 Luoshi Road, 430070 Wuhan, Hubei, China.

[b] Nanostructure Research Centre, Wuhan University of Technology, 122 Luoshi Road, 430070 Wuhan, Hubei, China.

[c] EMAT (Electron Microscopy for Materials Science), University of Antwerp, 171 Groenenborgerlaan, B-2020 Antwerp, Belgium.

[d] Laboratory of Inorganic Materials Chemistry (CMI), University of Namur, 61 rue de Bruxelles, B-5000 Namur, Belgium.

[e] Clare Hall, University of Cambridge, Herschel Road, Cambridge CB3 9AL, United Kingdom.

[*]To whom correspondence should be addressed. Email: yu.li@whut.edu.cn, minwu@whut.edu.cn, baoliansu@whut.edu.cn and bao-lian.su@unamur.be

Abstract

The slow photon effect, a structural effect of photonic crystal photocatalyst, is very efficient in the enhancement of photocatalytic reactions. However, slow photons in powdered photonic crystal photocatalyst have rarely been discussed because they are usually randomly oriented when the photocatalytic reaction happens in solution under constant stirring. In this work, for the first time we design a gradient ternary TiO_2-Au-CdS photonic crystal based on three-dimensionally ordered macroporous (3DOM) TiO_2 as skeleton, Au as electron transfer medium and CdS as active material for photocatalytic H_2 production under visible-light. As a result, this gradient ternary photocatalyst is favorable to simultaneously enhance light absorption, extend the light responsive region and reduce the recombination rate of the charge carriers. In particular, we found that slow photons at blue-edge exhibit much higher photocatalytic activity than that at red-edge. The photonic crystal photocatalyst with a macropore size of 250 nm exhibits the highest visible-light H_2 production rate of 3.50 $mmolh^{-1}g^{-1}$ due to the slow photon energy at the blue-edge to significantly enhance the incident photons utilization. This work verifies that slow photons at the blue-edge can largely enhance light harvesting and sheds a light on designing the powdered photonic crystal photocatalyst to promote the photocatalytic H_2 production via slow photon effect.

Keywords: Gradient ternary 3DOM TiO_2-Au-CdS; photonic crystals; blue-edge; red-edge; slow photon effect; photocatalytic H_2 production

1. Introduction

Photonic crystals have been capturing growing interest in photocatalysis and photoelectrochemistry because of the light harvesting enhancement through the slow photon effect [1-4]. Three-dimensionally ordered macroporous (3DOM) structure, one of the representative photonic crystal skeletons, is widely used for enhancing the photocatalytic and photovoltaic cell efficiencies owing to the strong light harvesting effect [4-6]. Such 3DOM materials have a periodic dielectric contrast modulation of the refractive index on the length scale of the light wavelength, where light with certain energy is forbidden to propagate through the material along a particular crystallographic direction giving rise to a stop-band reflection (also called photonic band gap, PBG) [7-9]. Most importantly, at the edges of the PBG, photons propagate through the material with a strongly reduced group velocity, called slow photons, leading to a delay and residence of light inside the photonic crystals [10]. When the lower frequency edge (called red-edge) and/or the higher frequency edge (called blue-edge) of these slow photons overlaps with the electronic band gap (EBG) of the photonic crystal photocatalyst, a significant enhancement of the photocatalytic activity can be expected via the increased effective optical path length. Previous studies have shown that changing the incident angle, the filling fraction and the macropore size (also called air-sphere size) can tune the PBG and therefore largely increase the photocatalytic efficiency by the slow photon effect [10-15].

Slow photon enhanced photocatalytic efficiency has been observed for 3DOM structures composed of various components, such as TiO_2 [16-19], ZnO [20], WO_3 [21, 22] or heterostructures [23, 24]. For example, Wu *et al*. systematically investigated TiO_2 inverse opal with the effects of incident light angles and macropore sizes on the PBG [18]. Liu *et al*. revealed the enhanced photocatalytic performance of ZnO inverse opal by the slow photon effect when changing the incident light angle [20]. In these cases, slow photon effect is investigated in films as the adjustment of incident light angle could easily regulate the position of PBG [18-28]. However, this angle dependence is infeasible for powdered 3DOM structures due to the fact that powdered samples

would be randomly oriented during the photocatalytic reaction as the solution is constantly stirred. Therefore, a fine design of the powdered 3DOM structure is quite challenge to avoid the effect of lattice constant on reflectance spectrum according to the modified Bragg law [9, 29].

It is known that the electromagnetic field of slow photons at red-edge tends to concentrate in the high dielectric constant part of the skeleton while that at blue-edge would concentrate in the low dielectric constant part [2, 11, 13, 21, 30]. Recently, a theoretical study of Deparis *et al*. indicates that the blue-edge slow photons are also able to enhance light harvesting through rigorous couple wave analysis simulations [31]. This result is quite interesting. Generally, the slow photons at red-edge are believed to have more practical applications for photocatalytic reactions as light in the representative 3DOM structures is primarily localized in the high dielectric part of the photonic crystals. At the blue-edge of the PBG, light is localized in the low dielectric part (the voids of the 3DOM structure, usually filled with air or liquid) and is less involved in the photoreaction [8]. It is then worth distinguishing the enhancement of photocatalytic activity at the red-edge or blue-edge slow photons for photonic crystal photocatalyst.

Herein, considering the prominent properties of hierarchical 3DOM structure, we report the fine design of a gradient ternary powdered 3DOM TiO_2-Au-CdS (TAC) photonic crystal photocatalyst for the visible-light-driven H_2 production by the slow photon effect from red-edge and blue-edge. In this gradient ternary composite, TiO_2 provides the 3DOM structure for a better light penetration and mass transfer, while CdS is the visible-light responsive component. This forms a heterostructure for efficient separation of the photogenerated carriers. In addition, Au nanoparticles (Au NPs) serve as the electron-transfer mediator to effectively separate the photogenerated electrons and holes [24]. Slow photon effect occurs via tuning the macropore size of photonic crystal skeleton to match the PBG of 3DOM TAC and the EBG of CdS. Our results show that slow photons at blue-edge in the gradient ternary 3DOM TAC demonstrate much higher influence on the photocatalytic H_2 production comparing to slow photons at red-edge. The present work proves the significant role of slow photons at blue-edge in the photocatalysis enhancement and demonstrates

an efficient design of powdered photonic crystal photocatalyst via slow photons to enhance H_2 production from visible-light-driven water splitting.

2. Experimental Section

2.1 Synthesis of polystyrene spheres and template preparation

A surfactant-free emulsion polymerization method is applied to prepare polystyrene (PS) spheres. Typically, styrene is washed several times using 2M NaOH to remove the inhibitors. PS spheres with different sizes are fabricated through changing the temperature, the concentration of styrene and the amount of initiator. For example, 330 nm PS spheres are synthesized as follows: prewashed styrene (30 ml) and water (400 ml) are heated to 80 ^{o}C in an oil bath under N_2 atmosphere. The initiator $K_2S_2O_8$ (0.3 g) is added to activate the polymerization. The reaction is stopped by cooling the container after stirring for 5 h. A PS colloidal template is obtained via oven-drying PS spheres monodispersed in water at certain concentration through controlling the drying speed at 40 ^{o}C.

2.2 Preparation of 3DOM TiO_2

The preparation of the 3DOM TiO_2 is according to our previous report [11]. The precursor is composed of ethanol (5 ml), hydrochloric acid (1 ml), titanium (IV) isopropoxide (5 ml), and water (2 ml). The mixture is added to a beaker and stirred at room temperature for 5 mins. A dried PS template (5 g) is placed on a filter paper in a Buchner funnel and the precursor is added to the PS templates during suction applied to the Buchner funnel. After air-drying the mixture of precursor and template for 48 h, calcination in air is applied to remove the PS template. The sample is stabilized at 300 ^{o}C for 2 h, 400 ^{o}C for 2 h and 550 ^{o}C for 2 h using a heating rate of 2 ^{o}C/min.

2.3 Decoration of Au nanoparticles on the 3DOM TiO_2

Au NPs are prepared by citrate reduction of $HAuCl_4$ in water. Typically, $HAuCl_4$ aqueous solution (10^{-2} g/L) is heated to 110 ^{o}C and 1.5 ml trisodium citrate aqueous solution (10 g/L) is added to the flask and another 1.5 ml is added after 15 mins. The mixture is stirred for 1 h at 110 ^{o}C

and cooled down to room temperature. 3DOM TiO_2 is then immersed into the Au NPs aqueous solution and the dark purple 3DOM TiO_2-Au is obtained after oven-drying the mixture.

2.4 Fabrication of 3DOM TiO_2-Au-CdS (3DOM TAC)

The 3DOM TAC samples are prepared by the chemical bath deposition method. Typically, the 3DOM TiO_2-Au sample is dipped in a 0.05 M $Cd(NO_3)_2$ aqueous solution for 5 min and then transferred to a 0.05 M Na_2S aqueous solution for 5 min. The above procedure is repeated for three times. The 3DOM TiO_2-Au-CdS is obtained after filtration and washed with deionized (DI) water. The as-fabricated samples are designated as 3DOM TAC-x (x is the macropore size measured from the SEM results).

2.5 Characterizations

The morphology and structure of the 3DOM TAC are observed by field-emission scanning electron microscopy (SEM, Hitachi S-4800) and transmission electron microscopy (TEM, JEOL JEM 2100F). High angle annular dark field-scanning transmission electron microscopy (HAADF-STEM) and energy-dispersive X-ray spectroscopy (EDX) are acquired on the bronze microgrids with the honey carbon film by using a FEI Titan 80-300 Themes microscope with double-aberration corrector and a Super-X windowless EDX detector. The crystal structure of the samples is examined by powder X-ray diffraction (XRD, D8 ADVANCE) at 40 kV, 40 mA equipped with a Cu anode X-ray tube (Cu Kα X-rays, λ=1.54056 Å). The Brunauer-Emmett-Teller (BET) specific surface areas of the powders were analyzed in a Micrometrics Tri Star II 3020 nitrogen adsorption-desorption apparatus. The UV-Vis absorption spectra are collected by SHIMADZU UV-Vis spectrophotometer in the range of 200-800 nm with $BaSO_4$ as the reference. The photoluminescence (PL) spectra are recorded using fluorescence spectrophotometer (PerkinElmer LS-55) and the excitation wavelength is set at 300 nm. The reflectance spectra are measured by Avaspec 2048/2 fiber-optic spectrometer in the range of 200-1100 nm. The electrochemical impedance spectroscopy (EIS) was performed on an electrochemical workstation (Autolab PGSTAT 302N) in the frequency range from 100 kHz to 10 mHz in a standard three-electrode system using the as-fabricated photocatalyst films as the

working electrodes, a Pt plate electrode as the counter electrode and a Ag/AgCl (saturated in KCl) as the reference electrode. Transient photocurrent response *vs* time was measured in 0.5 mol/L Na_2SO_4 electrolyte with light on/off cycles for different ternary samples under visible light irradiation at bias of 0 V vs Ag/AgCl.

2.6 Photocatalytic H_2 production

The photocatalytic reactions are carried out in a closed circulation system (Beijing Perfectlight Science & Technology Co., LTD) using a PLS-SXE-300C lamp with a visible-light intensity of 158 mW/cm^2. Typically, 0.1 g sample is immersed in an aqueous solution containing 0.1 M Na_2S and 0.1 M Na_2SO_3 as the sacrificial agents. The mixture is sealed in a quartz vessel and stirred during photoreaction. After degassing, the vessel is under irradiation of visible-light ($\lambda \geq 420$ nm). The gas products are analyzed periodically by an Agilent 7890A gas chromatograph (GC) with a thermal conductivity detector (TCD).

3. Results and Discussions

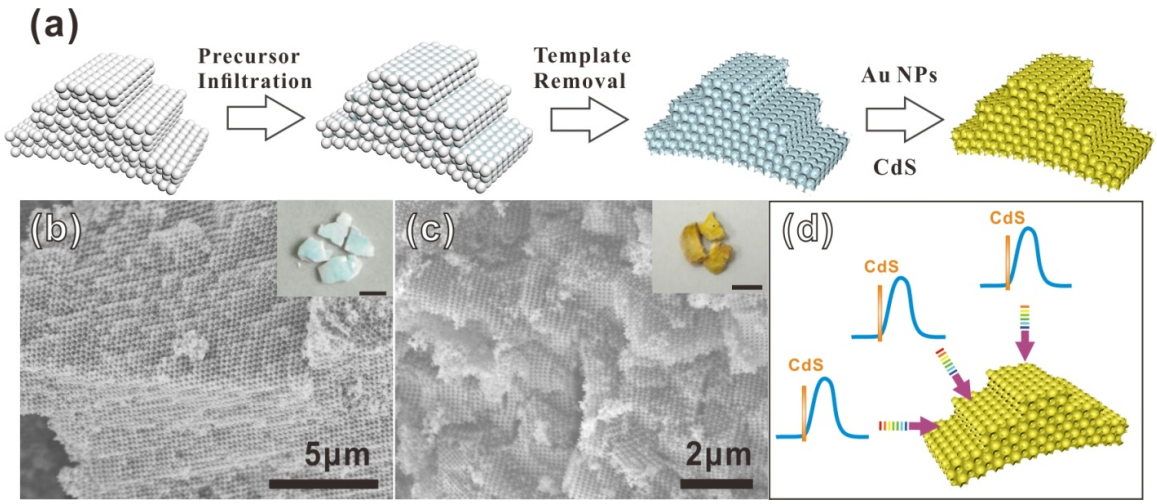

Figure 1. (a) Schematic illustration of the fabrication process of 3DOM TAC, (b) SEM images of 3DOM TiO_2-250, (c) SEM images of 3DOM TAC-250 and (d) schematic illustration of light reflection simulation of 3DOM TAC at different incident angles. The insets in (b) and (c) are the corresponding photographs, scale bar = 5 mm.

Figure 1a illustrates the fabrication process of the gradient ternary powdered 3DOM TAC photonic crystal photocatalyst. The monodispersed PS spheres are firstly self-assembled into closely

packed photonic crystals with gradient stage by controlling water evaporation. Note that the evaporation speed is very important for gradient stage formation. The titanium precursor is then penetrated into the PS template and hydrolyzed in the interspace. After calcination in air, 3DOM TiO_2 structure is obtained (Figure 1b). For example, the as-fabricated 3DOM TiO_2-250 gives a specific green structure-color related to the configuration, incident light angle and macropore size (Figure 1b inset). This green structure color indicates the good quality of inverse opal structure. The SEM images and corresponding photographs of 3DOM TiO_2 with different macropore sizes are shown in Figure S1. These structure colors are consistent with the reflectance spectra measured in air (Figure S2). After the introduction of Au NPs and CdS, the green structure-color of 3DOM TiO_2-250 (Figure 1c inset and Figure S1e-h) turns to the intrinsic yellow color of CdS for 3DOM TAC-250. It is worth noting that all the as-fabricated samples have a gradient face-centered-cubic structure upon the intensive SEM observations (Figure 1b and c). This unique structure in powdered photonic crystals can maintain the reflectance property at different incident light angles and decrease the effect of random orientation during the photocatalytic reaction when the solution is constantly stirred as schemed in Figure 1d. Back scattered electron (BSE) images are further conducted to reveal the dispersion of the Au NPs in 3DOM TAC samples. Figure S3 shows the BSE image of 3DOM TAC-250. It clearly displays that Au NPs are well dispersed in the skeleton of 3DOM TAC-250.

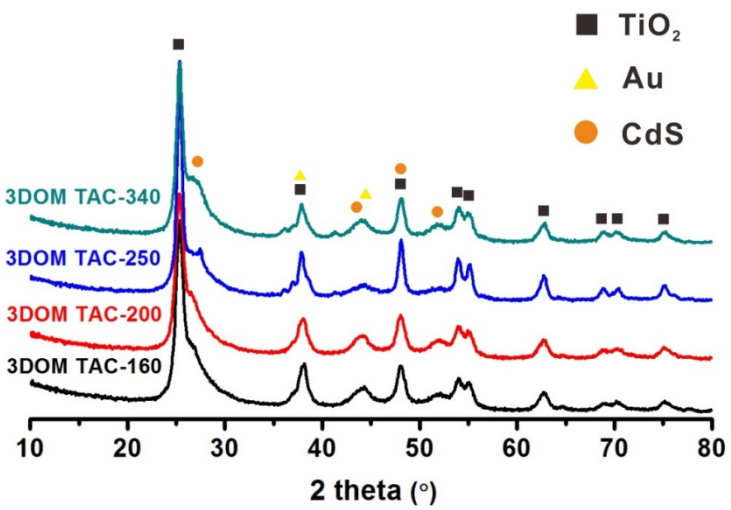

Figure 2. XRD patterns of 3DOM TAC with different pore sizes.

Figure 2 shows the XRD patterns of the 3DOM TAC samples with different macropore sizes. The characteristic diffraction peaks of TiO_2 indicate a pure anatase phase. The average crystallite size of TiO_2 is approximately 10 nm according to the Scherrer's equation [32]. The deposited CdS presents the greenockite phase with crystallographically preferred orientations. The peaks at 38.2° and 44.4° correspond to Au (111) and (200), indicating a successful decoration by the Au NPs.

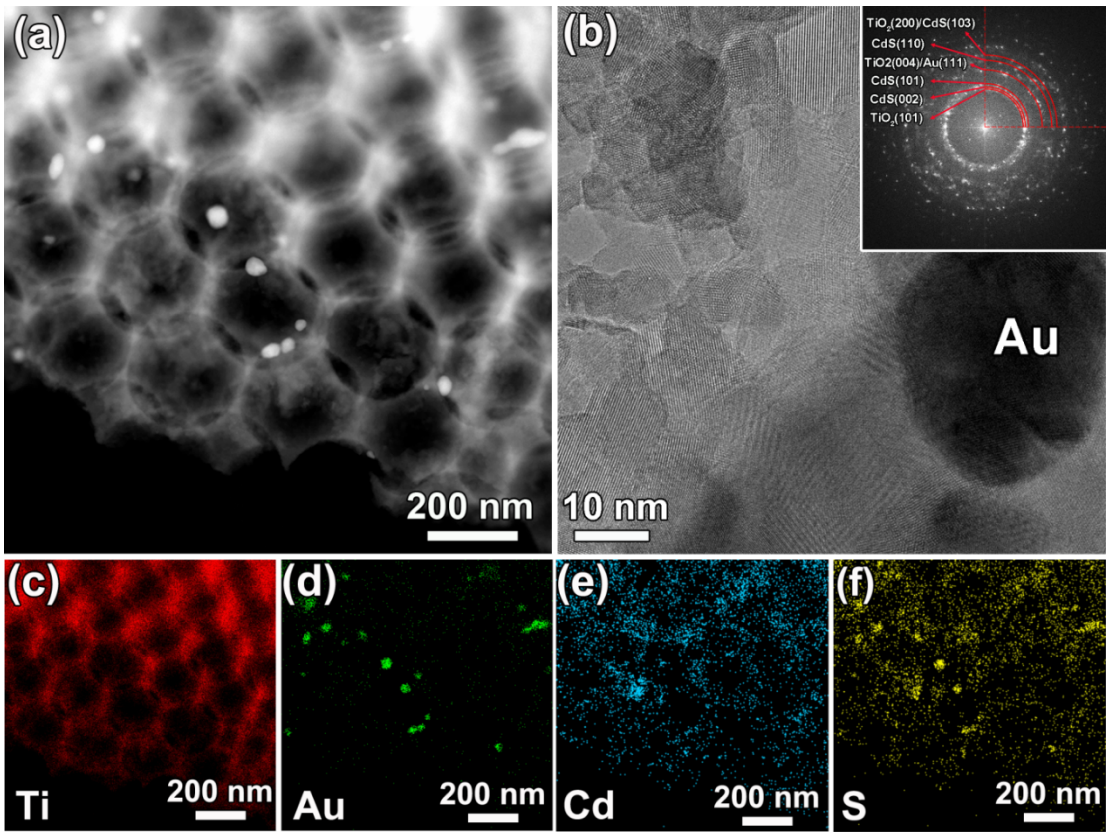

Figure 3. The TEM images of 3DOM TAC-250. (a) a typical HAADF-STEM image, (b) HRTEM image and corresponding FFT image of the whole area and (c-f) EDX elemental mapping images of the same area in a (Ti: red, Au: green, Cd: cyan and S: yellow). The inset in (b) is the corresponding SAED patterns in whole area.

The morphology and structure of 3DOM TAC are further characterized by TEM and STEM. Figure 3 shows a typical HAADF-STEM image of 3DOM TAC-250. It displays that the 3DOM structure is kept completely after the introduction of Au NPs and CdS. The crystallinity and intimate contacts of these three components can be identified from HRTEM and selected area electron diffraction (SAED) patterns (Figure 3b), indicating the formation of heterojunction. The crystalline grains sizes are shown in Table 1 which is the statistical results from 100 crystalline

grains of each component. Au NPs with the large size around 30 nm are uniformly distributed in the skeleton, consistent with BSE image shown in Figure S3. The corresponding EDX elemental mappings (Figure 3c-f) reveal the homogeneous distribution of Au NPs and CdS in 3DOM TiO_2, providing a strong evidence for the formation of ternary hybrid heterojunctions. Such heterojunctions in 3DOM TAC can effectively separate the photogenerated carrier charges, facilitate the photogenerated electrons transfer from CdS to TiO_2, thus finally prolong the lifetime of charge carriers and improve photocatalytic activity [24, 33], which could be further revealed by the electrochemical impedance spectroscopy (EIS) result as shown in Figure S4.

Table 1 The structure parameters of TAC and 3DOM TAC with different pore sizes.

Sample	Macropore size/nm	Crystalline grains size/nm			S_{BET}/m^2g^{-1}	Mesopore size/nm
		TiO_2	Au	CdS		
TAC	-	11±3	30±5	10±3	37.6	2.2, 10.7
3DOM TAC-160	160±5	9±3	30±5	11±3	24.5	2.1
3DOM TAC-200	200±5	10±3	29±5	10±3	26.4	2.3
3DOM TAC-250	250±5	10±3	30±5	11±3	28.1	2.4
3DOM TAC-340	340±5	9±3	31±5	10±3	24.5	2.3

It is known that the macropore size and refractive index can determine the reflectance property of photonic crystal photocatalyst with different components. In these ternary composites, the small crystallites of CdS cannot affect the macropore size as evidenced by SEM observation. On the other hand, both the refractive indices of anatase TiO_2 and CdS are approximate to 2.5. Figure 4a shows the reflectance spectra of 3DOM TiO_2, 3DOM TiO_2-Au and 3DOM TiO_2-Au-CdS with 340 nm macropore size measured in water. As expected, the result shows that the incorporation of Au NPs and small CdS crystallites in 3DOM TiO_2 cannot change the PBG, similar to the previous report [27]. Therefore, changing the macropore size of the ternary composite can tune the PBG of the powdered 3DOM TAC as illustrated in Figure 4b. The good shape of reflectance spectra indicates the high quality inverse opal structure over a long range. And the positions of stop-bands red-shift owing to the larger macropores packed with a larger lattice constant [23]. When the energy at the red-edge and/or blue-edge of the PBG overlaps with the EBG of CdS, slow photons can occur to enhance the electron excitation from the valence band (VB) to the conduction band (CB) of CdS.

The photocatalytic activity is then greatly improved. The light absorption spectra of all as-fabricated 3DOM TAC samples are demonstrated in Figure S5. It shows that all the samples have similar intrinsic absorption of TiO_2 and CdS in the range of 300-800 nm. This indicates that the surface plasmonic resonance (SPR) absorption in the CdS-Au-TiO_2 ternary system is too weak to negligible. This result is consistent with our previous work [34], where the photocatalytic H_2 evolution under monochromatic light has proved that the photocatalytic enhancement of the plasmonic effect of Au NPs with 30 nm is negligible. From the absorption spectra, one can see that the EBG of CdS is ~2.40 eV (Figure S6), corresponding to a wavelength at ~520 nm (orange dotted line in the inset of Figure 4b sampled by 3DOM TAC-250). The shaded region corresponding to the electronic excitation wavelength of CdS overlaps the reflectance peak of 3DOM TAC-200, the red-edge of 3DOM TAC-160 and the blue-edge of 3DOM TAC-250. This is very suitable to show the slow photon effect on photocatalytic H_2 production for these samples.

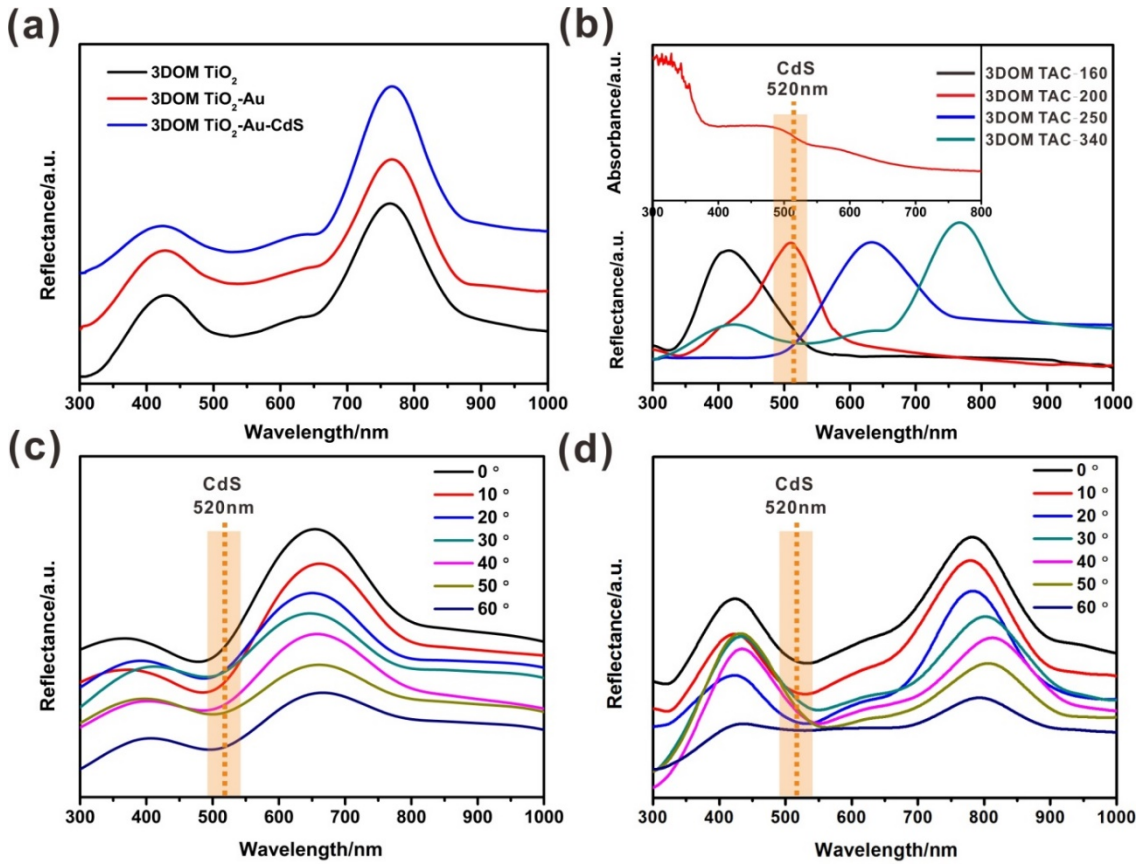

Figure 4. Light reflectance spectra of (a) 3DOM TiO_2, 3DOM TiO_2-Au and 3DOM TiO_2-Au-CdS with 340 nm macropore size, (b) 3DOM TAC with different pore sizes, (c) 3DOM TAC-250 and (d) 3DOM TAC-340 at different incident light angles.

As mentioned above, during the photocatalytic reaction, powdered samples in solution would be randomly oriented because of the constant stirring. To illustrate the effect of incident light angles on the reflectance of the as-fabricated gradient ternary powdered 3DOM TAC photocatalysts, light reflectance spectra of 3DOM TAC-250 and 3DOM TAC-340 randomly dispersed in glass slide at different incident light angles are measured, respectively (Figure 4c-d). The results reveal that changing light angle cannot affect the PBG of the two samples and their blue- and/or red-edges of the first-order and second-order reflectance locate at the same region. This should be attributed to the unique gradient structure, which decreases the effect of random orientation, leading to the reflection spectra maintained at almost the same position with the incident angle change as shown in Figure 1d. Therefore, slow photons can always happen in such powdered samples for photocatalytic H_2 production.

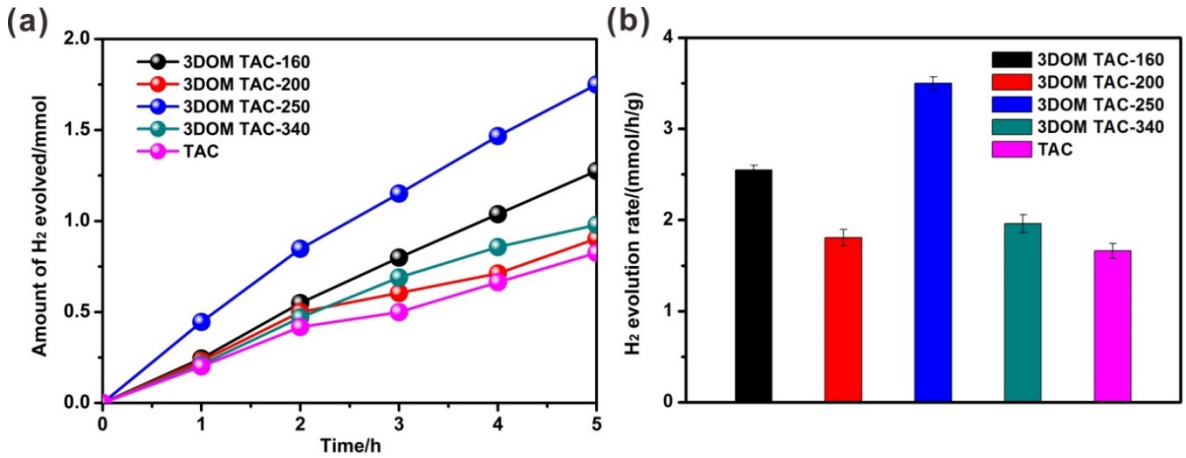

Figure 5. (a) H_2 production and (b) the corresponding H_2 production rates of TAC without a 3DOM structure and the gradient ternary 3DOM TAC photocatalysts under visible-light.

Visible-light-driven ($\lambda \geq 420$nm) water splitting for H_2 production is then performed to investigate the photocatalytic activities of the 3DOM TAC samples, especially to distinguish the red-edge and/or blue-edge slow photon effect for H_2 production. Figure 5a displays the photocatalytic activity of the gradient ternary 3DOM TAC with different macropore sizes. The specific values could be referred by Table S2. As a comparison, TAC without a 3DOM structure is also conducted. It shows that the 3DOM TAC photocatalysts possess better H_2 production abilities than TAC without a 3DOM structure even the later sample possesses larger specific surface area

(Table 1). As 3DOM structure has the interconnected hierarchically macro-mesoporous structure, this can ensure 3DOM TAC photocatalysts with excellent mass transfer property according to the established relation between the hierarchically porous structure and the mass transfer ability based on the general Murray law [35]. Meanwhile, the unique periodic dielectric structure gives rise to light multiple scattering and reflecting and even the potential slow photon effect. Therefore, more incident photons are absorbed by CdS to generate more charge carriers, consistent with the following PL results. This leads to enhanced photocatalytic activity. For example, although the PBG of 3DOM TAC-200 overlaps the EBG of CdS, this means that many incident photons can be reflected. As the result, 3DOM TAC-200 has much lower photocatalytic activity than other 3DOM TAC samples. However, 3DOM TAC-200 still exhibits better performance (1.8 $mmolh^{-1}g^{-1}$) than TAC without 3DOM structure (1.6 $mmolh^{-1}g^{-1}$) due to the easy mass transfer of macropore and the enhancement of incident photons absorption by the multiple scattering and reflecting.

As 3DOM TAC samples have almost the same specific surface areas, crystalline grains size and the mesoporous distributions (Table 1), the differences in H_2 evolution rates caused by the number of active sites could be eliminated. According to the UV-Vis reflectance spectra (Figure 4b), the red-edge of 3DOM TAC-160 and the blue-edge of 3DOM TAC-250 couple well with the electronic excitation wavelength of CdS. This leads to higher photocatalytic activity than other samples due to the slow photon effect. From Figure 5a, one can see that the blue-edge slow photon enhancement for H_2 production is much higher than the red-edge slow photon. The H_2 production rate of 3DOM TAC-250 is about 3.50 $mmolh^{-1}g^{-1}$, which is much higher than previous reported studies (Table S3). This result seems inconsistent with the conventional concept that the red-edge slow photon effect has more practical application for photocatalytic reactions as the slow photons directly interact with materials while the blue-edge slow photons concentrate in the low dielectric constant part. As slow photons are related to the PBG and EBG of semiconductor photonic crystals, the reflectance spectra of the two composites should give detailed information for this phenomenon (Figure 4b). For 3DOM TAC-160, its red-edge reflects more photons with high energies

(wavelength ≤ 520 nm). Namely many photons with high energies cannot be absorbed by 3DOM TAC-160. While for 3DOM TAC-250, the reflected photons with low energies (wavelength ≥ 520 nm) cannot activate CdS to generate charge carriers. Namely the photons with high energies can be fully absorbed by 3DOM TAC-250. As a result, 3DOM TAC-250 with blue-edge slow photon effect gives higher H_2 production than 3DOM TAC-160 with red-edge slow photon effect.

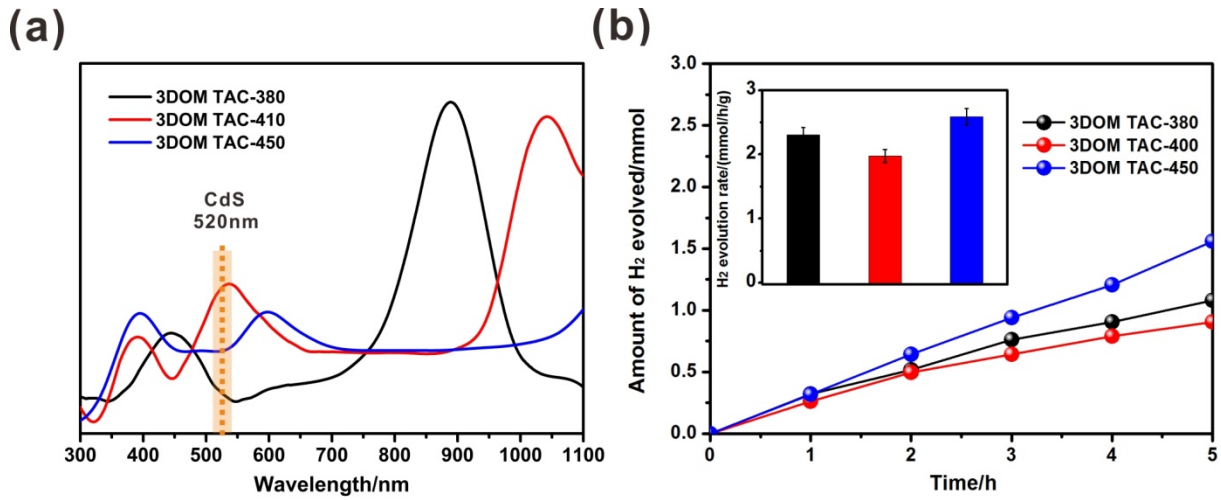

Figure 6. (a) Light reflectance spectra and (b) H_2 evolution of 3DOM TAC-380, 3DOM TAC-410 and 3DOM TAC-450.

In Figure 4b, it also reveals that the red-edge at the second-order reflection peak of 3DOM TAC-340 almost matches with the EBG of CdS. The photocatalytic H_2 production rate of 3DOM TAC-340 is also higher than those of 3DOM TAC-200 and TAC (Figure 5). Therefore, the improvement of second-order reflection peaks with slow photon effect at the red-edge and blue-edge is also conducted. Figure 6 presents the reflectance spectra for 3DOM TAC-380, 3DOM TAC-410 and 3DOM TAC-450. Compared with the first-order reflection, the second-order reflection peaks have much lower intensity [36], indicating more photons can reach the surface of the photocatalysts. The reflection curves show that the EBG of CdS overlaps the red-edge of 3DOM TAC-380, the reflection peak of 3DOM TAC-410 and blue-edge of 3DOM TAC-450, respectively. Again, the hydrogen production rates of these samples prove that the enhancement of photocatalytic activity at blue-edge slow photons from the second-order PBG is higher than that at the red-edge slow photons.

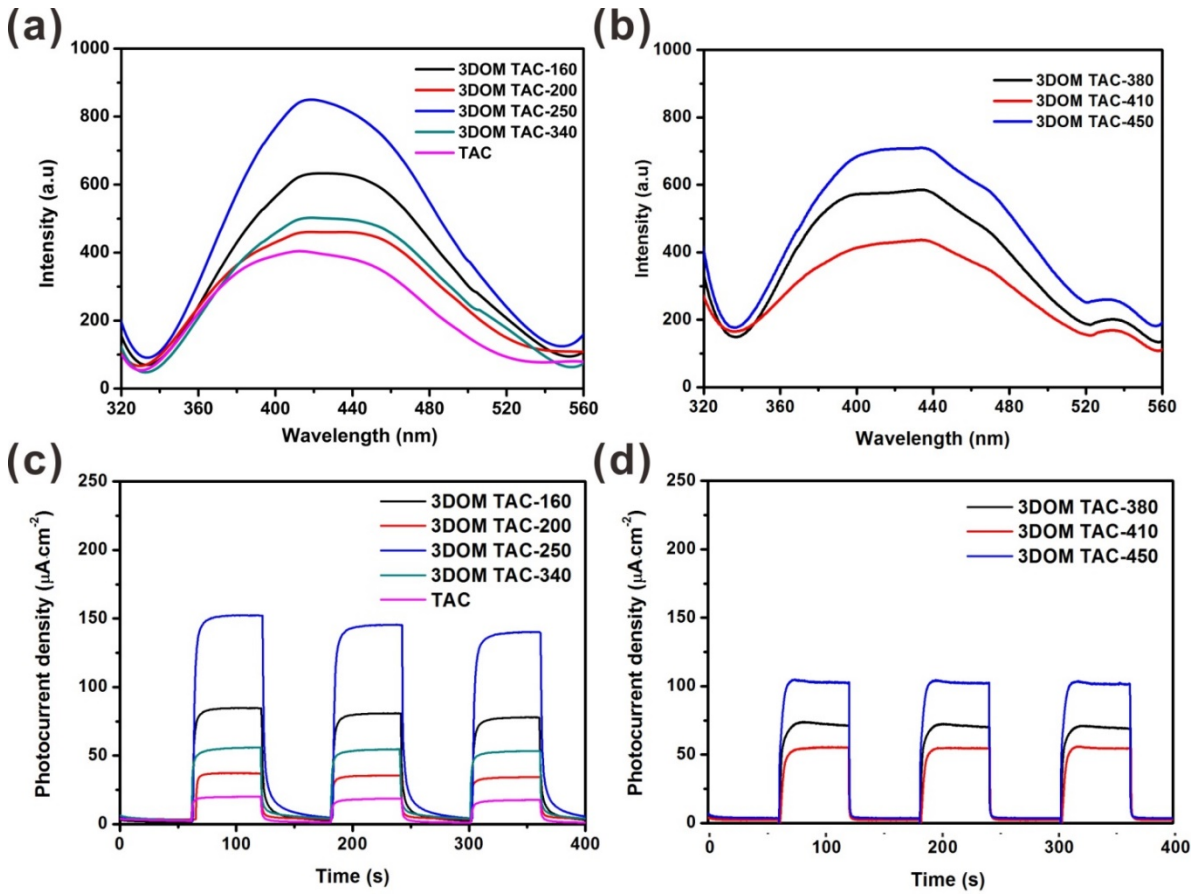

Figure 7. (a,b) PL spectra and (c,d) transient photocurrent of 3DOM TAC with different pore sizes.

To further reveal the better enhancement by the blue-edge slow photon effect, PL spectra of the 3DOM TAC photocatalysts are measured. Generally, the PL signal is generated from the recombination of electrons and holes. The PL intensity represents the recombination rate and (or) the number of photogenerated electrons and holes. As all ternary photocatalysts have the same components and heterojunction structure, we believe all ternary samples have the same separation efficiency of photogenerated charge carriers. Therefore, the PL intensity in this case could be on behalf of the number of photogenerated charge carriers in these samples [37, 38]. Figure 7a and 7b show the PL spectra of all samples measured with the excitation wavelength of 300 nm. Comparing to TAC, all the 3DOM TAC samples show the improved density of photogenerated charge carriers, indicating that the 3DOM structure is beneficial for photocatalysis. In particular, 3DOM TAC-160 and 3DOM TAC-250 demonstrate higher density of photogenerated charge carriers than other samples (Figure 7a), indicating higher light absorption due to slow photon effect. Meanwhile, the blue-edge slow photon effect in 3DOM TAC-250 shows higher intensity of charge carriers than the

red-slow photon effect in 3DOM TAC-160. Figure 7b also shows the same tendency for the 3DOM TAC photocatalysts with the second-order slow photon effect. Again, 3DOM TAC-450 at the blue-edge slow photon effect displays higher intensity of charge carriers than 3DOM TAC-380 at the red-edge slow photon. In addition, the relative PL intensity of each photocatalyst is consistent with the corresponding H_2 production rate. In order to demonstrate that the PL intensity could represent the number of photogenerated charge carriers for these ternary samples, the photocurrent was also measured as shown in Figure 7c and 7d. Apparently, the samples with 3DOM structure have much higher photocurrent densities than the sample without 3DOM structure, revealing that the 3DOM structure contributes to enhance the light absorption efficiency. In addition, the photocurrent densities of samples with different pore sizes are consistent with the PL intensities and photocatalytic H_2 evolution rates, demonstrating that the PL intensity indeed represents the number of photogenerated charge carriers in this case.

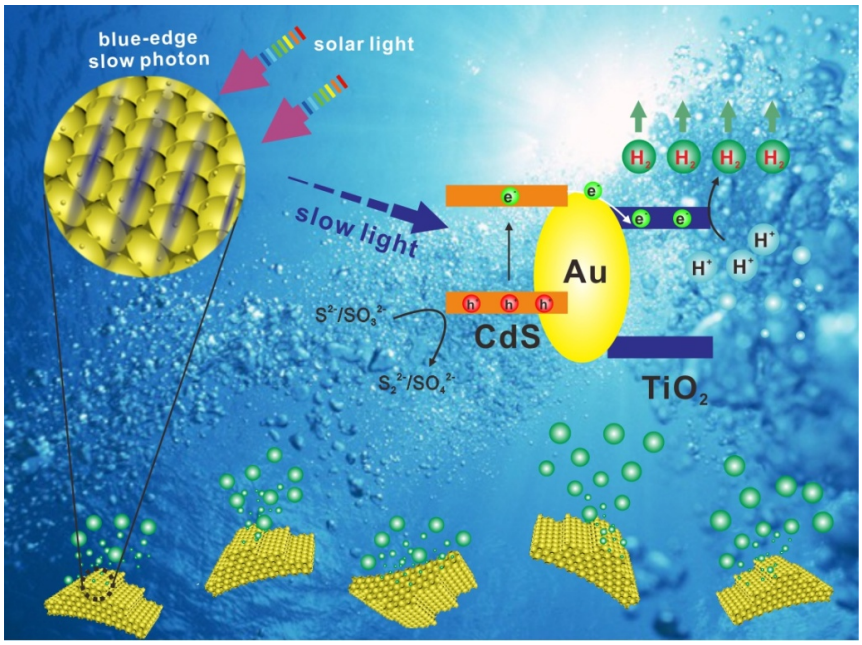

Figure 8. Schematic illustration of the slow photon effect in the gradient ternary powdered 3DOM TAC photonic crystal photocatalyst for H_2 production under visible-light.

Figure 8 illustrates the slow photon effect in the gradient ternary powdered 3DOM TAC photonic crystals for H_2 production under visible-light. Three steps proceed for the photocatalytic H_2 production [38]: (1) the incident light is absorbed by CdS to generate electrons and holes; (2) the photogenerated electrons transfer from the CB of CdS to the CB of TiO_2 via Au NPs; (3) the

electrons in the CB of TiO_2 reduce H^+ to produce H_2, whereas the holes in the VB of CdS induce the oxidation reaction. Generally, step (1) directly determines the H_2 production rate for the 3DOM TAC samples. As mentioned above, the samples with slow photon effect favor to generate more charge carriers and the blue-edge slow photon effect is more beneficial for H_2 production comparing to the red-edge slow photon effect. This helps to guide the synthesis of the gradient ternary powdered 3DOM photonic crystals for photocatalysis using the slow photon effect.

4. Conclusions

A visible-light responsive ternary powdered 3DOM-based heterostructure TiO_2-Au-CdS with gradient structure has been successfully fabricated by depositing Au NPs as electron transfer medium and CdS as active material onto the framework of 3DOM TiO_2. The gradient ternary photocatalysts exhibit highly enhanced performance for H_2 production under visible-light because of the light harvesting promotion by the slow photon effect and the efficient separation of photogenerated carriers via Au NPs. The energies of the slow photons are controlled by changing the macropore size to overlap the electronic excitation wavelength of CdS. The 3DOM TAC-250 sample exhibits outstanding photoreactivity (3.50 $mmolh^{-1}g^{-1}$) because of the slow photon enhancement at the blue-edge. This result proves that the blue-edge slow photon possesses ability in amplifying the photocatalytic reaction. The use of the blue-edge slow photons in the construction of photonic crystal-based heterostructures broadens the application field of the slow photon effect. It also sheds a new light onto future studies of the slow photon effect for large-scale H_2 production from visible-light-driven water splitting.

Acknowledgements

B. L. Su acknowledges the Chinese Central Government for an “Expert of the State” position in the Program of the “Thousand Talents”. Y. Li acknowledges Hubei Provincial Department of Education for the “Chutian Scholar” program. This work is financially supported the National Key

R&D Program of China (2016YFA0202602), National Natural Science Foundation of China (U1663225, 51502225), Program for Changjiang Scholars and Innovative Research Team in University (IRT_15R52), Hubei Provincial Natural Science Foundation (2015CFB516), International Science &Technology Cooperation Program of China (2015DFE52870) and the Fundamental Research Funds for the Central Universities (WUT: 2016III029).

References

[1] J. Liu, H. Zhao, M. Wu, B. Van der Schueren, Y. Li, O. Deparis, J. H. Ye, G. A. Ozin, T. Hasan, B. L. Su, Adv. Mater. 29 (2017) 1605349.

[2] X. Zhang, Y. Liu, S. T. Lee, S. H. Yang, Z. H. Kang, Energ. Environ. Sci. 7 (2014) 1409-1419.

[3] G. von Freymann, V. Kitaev, B. V. Lotsch, G. A. Ozin, Chem. Soc. Rev. 42 (2013) 2528-2554.

[4] A. Stein, B. E. Wilson, S. G. Rudisill, Chem. Soc. Rev. 42 (2013) 2763-2803.

[5] X. Y. Yang, L. H. Chen, Y. Li, J. C. Rooke, C. Sanchez, B. L. Su, Chem. Soc. Rev. 46 (2017) 481-558.

[6] M. H. Sun, S. Z. Huang, L. H. Chen, Y. Li, X. Y. Yang, Z. Y. Yuan, B. L. Su, Chem. Soc. Rev. 45 (2016) 3479-3563.

[7] E. Yablonovitch, Phys. Rev. Lett. 58 (1987) 2059-2062.

[8] S. Nishimura, N. Abrams, B. A. Lewis, L. I. Halaoui, T. E. Mallouk, K. D. Benkstein, J. van de Lagemaat, A. J. Frank, J. Am. Chem. Soc. 125 (2003) 6306-6310.

[9] M. M. Ren, R. Ravikrishna, K.T. Valsaraj, Environ. Sci. Technol. 40 (2006) 7029-7033.

[10] J. I. L. Chen, G. von Freymann, S. Y. Choi, V. Kitaev, G. A. Ozin, Adv. Mater. 18 (2006) 1915-1919.

[11] M. Wu, Y. Li, Z. Deng, B. L. Su, ChemSusChem. 4 (2011) 1481-1488.

[12] Q. Yang, M. Li, J. Liu, W. Shen, C. Ye, X. Shi, L. Jiang, Y. Song, J. Mater. Chem. A 1 (2013) 541-547.

[13] J. I. L. Chen, G.A. Ozin, J. Mater. Chem. 19 (2009) 2675-2678.

[14] R. C. Schroden, M. Al-Daous, A. Stein, Chem. Mater. 13 (2001) 2945-2950.

[15] G. von Freymann, S. John, V. Kitaev, G. A. Ozin, Adv. Mater. 17 (2005) 1273-1276.

[16] J. Liu, G. L. Liu, M. Z. Li, W. Z. Shen, Z.Y. Liu, J.X. Wang, J.C. Zhao, L. Jiang, Y. L. Song, Energ. Environ. Sci. 3 (2010) 1503-1506.

[17] W. J. Hyun, H. K. Lee, S. S. Oh, O. Hess, C. G. Choi, S. H. Im, O. O. Park, Adv. Mater. 23 (2011) 1846-1850.

[18] M. Wu, J. Jin, J. Liu, Z. Deng, Y. Li, O. Deparis, B. L. Su, J. Mater. Chem. A 1 (2013) 15491-15500.

[19] M. Wu, J. Liu, J. Jin, C. Wang, S. Huang, Z. Deng, Y. Li, B. L. Su, Appl. Catal. B-Environ. 150 (2014) 411-420.

[20] J. Liu, J. Jin, Y. Li, H. W. Huang, C. Wang, M. Wu, L. H. Chen, B. L. Su, J. Mater. Chem. A 2 (2014) 5051-5059.

[21] X.Q. Chen, J. H. Ye, S. X. Ouyang, T. Kako, Z. S. Li, Z. G. Zou, ACS Nano 5 (2011) 4310-4318.

[22] H. Zhang, G. Duan, G. Liu, Y. Li, X. Xu, Z. Dai, J. Wang, W. Cai, Nanoscale 5 (2013) 2460-2468.

[23] X. F. Cui, Y. J. Wang, G. Y. Jiang, Z. Zhao, C. M. Xu, Y. C. Wei, A. J. Duan, J. Liu, J. S. Gao, RSC Adv. 4 (2014) 15689-15694.

[24] J. T. Li, S. K. Cushing, P. Zheng, T. Senty, F. K. Meng, A. D. Bristow, A. Manivannan, N. Q. Wu, J. Am. Chem. Soc. 136 (2014) 8438-8449.

[25] R. Fayad, L. Halaoui, ChemPhysChem. 17 (2016) 260-269.

[26] X. Li, X. Zhang, X. Zheng, Y. Shao, M. He, P. Wang, X. Fu, D. Li, J. Mater. Chem. A 2 (2014) 15796-15802.

[27] Z. Y. Cai, Z. G. Xiong, X. M. Lu, J. H. Teng, J. Mater. Chem. A 2 (2014) 545-553.

[28] L. Zhang, C. Y. Lin, V. K. Valev, E. Reisner, U. Steiner, J. J. Baumberg, Small 10 (2014) 3970-3978.

[29] F. Piret, B. L. Su, Chem. Phys. Lett. 457 (2008) 376-380.

[30] Y. Wang, D. B. Xiong, W. Zhang, H. Su, Q. Liu, J. Gu, S. Zhu, D. Zhang, Catal. Today 274 (2016) 15-21.

[31] O. Deparis, S. R. Mouchet, B. L. Su, Phys. Chem. Chem. Phys. 17 (2015) 30525-30532.

[32] H. Borchert, E. V. Shevehenko, A. Robert, I. Mekis, A. Kornowski, G. Grubel, H. Weller, Langmuir 21 (2005) 1931-1936.

[33] L. Q. Liu, S. X. Ouyang, J. H. Ye, Angew. Chem. Int. Edit. 52 (2013) 6689-6693.

[34] H. Zhao, M. Wu, J. Liu, Z. Deng, Y. Li, B. L. Su, Appl. Catal. B-Environ. 184 (2016) 182-190.

[35] X. F. Zheng, G. F. Shen, C. Wang, Y. Li, D. Dunphy, T. Hasan, C. J. Brinker, B. L. Su, Nat. Commun. 8 (2017) 14921.

[36] R. V. Nair, R. Vijaya, Phys. Rev. A 76 (2007) 053805.

[37] Y. Ma, X. L. Wang, Y. S. Jia, X. B. Chen, H. X. Han, C. Li, Chem. Rev. 114 (2014) 9987-10043.

[38] W. F. Zhang, M. S. Zhang, Z. Yin, Q. Chen, Appl Phys B-Lasers O 70 (2000) 261-265.

Heng Zhao received his Bachelor degree from Wuhan University of Technology majored in Applied Chemistry in 2013. He is currently a Ph.D. student in Wuhan University of Technology majored in Material Physics and Chemistry under guidance of Prof. Dr. Min Wu and Prof. Dr. Bao-Lian Su. His research mainly focuses on the design and synthesis of three-dimensionally ordered macroporous catalysts for the photocatalytic hydrogen generation.

Zhi-Yi Hu received his Bachelor degree in materials science and engineering and Master degree in materials science from Wuhan University of Technology in 2010 and 2012 respectively. He obatined his Ph.D. in physics from the University of Antwerp in 2016. He is currently a post-doctoral researcher in the electron microscopy group EMAT at the University of Antwerp. His research focuses on advanced electron microscopy for nanomaterials, including HR-TEM, HR-STEM, STEM-EDX, STEM-EELS and 3D electron tomography.

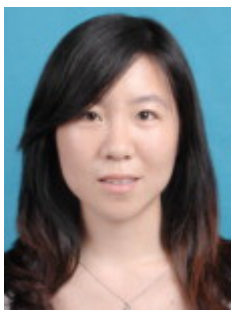

Jing Liu received her Ph.D. degree in Material Physics and Chemistry in 2016, Bachelor degree in Material Chemistry in 2010 and Master degree in Material Science in 2013 from the Wuhan University of Technology. Her current research interests are mainly focused on the photocatalysts for energy conversion.

Yu Li received his B.S. from Xi'an Jiaotong University in 1999 and received his M.S. from Liaoning Shihua University in 2002. He obtained his Ph.D. from Zhejiang University in 2005. He

worked in EMAT at the University of Antwerp with Prof. G. Vantendeloo in 2005 and then in CMI at the University of Namur with Prof. Bao-Lian Su in 2006. Currently, he is a “Chutian” Professor at Wuhan University of Technology. His research interests include nanomaterials design and synthesis, hierarchically porous materials synthesis, and their applications in the fundamental aspects of energy and environment.

Min Wu received her Bachelor and Master degrees from Wuhan University of Technology in Material Science and Engineering in 2005. She obtained her Ph.D in Physics from Institute of Photonics, University of Strathclyde, UK in 2010 and went to the University of Namur as a post-doctoral researcher in CMI Laboratory with Prof. Bao-Lian Su after. Currently, she is a Professor in Wuhan University of Technology and her research interests are inorganic semiconductor nanomaterials photonic crystals design and synthesis for photosynthesis and photocatalysis in environment and energy fields.

Gustaaf Van Tendeloo studied physics and graduated from the University of Antwerp in 1974. He is a professor at the University of Antwerp and part-time professor at the University of Brussels. He is the director of the electron microscopy group EMAT at the University of Antwerp. His research interests are focused on the application of advanced electron microscopy to different aspects of materials science. In 2009, he received an ERC Advanced Grant. In 2015, he won the FWO Excellence award (Dr. De Leeuw-Damry-Boulart award).

Prof. Bao-Lian Su created the Laboratory of Inorganic Materials Chemistry (CMI) at the University of Namur, Belgium in 1995. He is currently Full Professor of Chemistry, Member of the Royal Academy of Belgium, Fellow of the Royal of Society of Chemistry, UK and Life Member of Clare Hall College, University of Cambridge. He is also Changjiang Professor at Wuhan University of Technology and an “Expert of the State” in the frame of “Thousands Talents” program, China. His current research fields include the synthesis, the property study and the molecular engineering of organized, hierarchically porous and bio-organisms for artificial photosynthesis, (photo) Catalysis, Energy Conversion and Storage, Biotechnology, Cell therapy and Biomedical applications.

Supporting Information

Blue-edge Slow Photons Promoting Photocatalytic Hydrogen Evolution of Ternary 3DOM TiO_2-Au-CdS Photonic Crystals

Heng Zhao[a], Zhiyi Hu[a,b], Jing Liu[a], Yu Li[a*], Min Wu[a*], Gustaaf Van Tendeloo[b,c], Bao-Lian Su[a,d,e*]

[a] State Key Laboratory of Advanced Technology for Materials Synthesis and Processing, Wuhan University of Technology, 122 Luoshi Road, 430070 Wuhan, Hubei, China.

[b] Nanostructure Research Centre, Wuhan University of Technology, 122 Luoshi Road, 430070 Wuhan, Hubei, China.

[c] EMAT (Electron Microscopy for Materials Science), University of Antwerp, 171Groenenborgerlaan, B-2020 Antwerp, Belgium.

[d] Laboratory of Inorganic Materials Chemistry (CMI), University of Namur, 61 rue de Bruxelles, B-5000 Namur, Belgium.

[e] Clare Hall, University of Cambridge, Herschel Road, Cambridge CB3 9AL, United Kingdom.

[*]To whom correspondence should be addressed. Email: yu.li@whut.edu.cn, minwu@whut.edu.cn, baoliansu@whut.edu.cn and bao-lian.su@unamur.be

Theoretical Calculation of PBG

As semiconductors have an electronic bandgap (EBG), photonic crystals have a photonic bandgap (PBG), which can be tuned by varying the pore sizes according to a modified Bragg law.

(1)

(2)

In these equations, λ_p is the wavelength of peak derived from the stop-band, d_{hkl} is the lattice constant, m is the order of Bragg diffraction, n_{eff} is the average refractive index of 3DOM TAC, θ is the angle of the incident light to the plane, n_{solid} and n_{void} are the refractive indices of the solid (TiO_2 and CdS, the contribution of Au NPscan be eliminated due to low content in ternary 3DOM TAC) and the void (filled by water in this case), respectively, φ is the solid volume percentage. For a face-centered-cubic structure, the first-order diffractionis from the (111) planes, m=1 and d_{111}=0.816D, D is the diameter of the macropore. The refractive index of anatasen_{TiO2}=2.55, n_{CdS}=2.51, n_{H2O}=1.33. Thus, we approximate n_{solid}at 2.5 due to the similar indices between TiO_2 and CdS. $\varphi$is generally taken as 0.26 for the complete inverse opal structure. Therefore, formula (1) transforms to:

(3) $\lambda_p = 1.632D\ (1.634^2 - \sin^2\theta)^{1/2}$

Due to the stirring reaction system and powdered sample used, the incident angle θ for a given piece of sample changes constantly during the reaction. Fortunately, the incident angle is proved to slightly affect the reflectance property of the as-fabricated samples. Powder photonic crystals with various pore sizes exhibit different colors caused by the 3DOM structureand the pore size (D) is an extremely important parameter determining the energy of the slow photons. Details on the calculated and measured PBG of 3DOM TACwith different pore sizes are shown in Table S1.

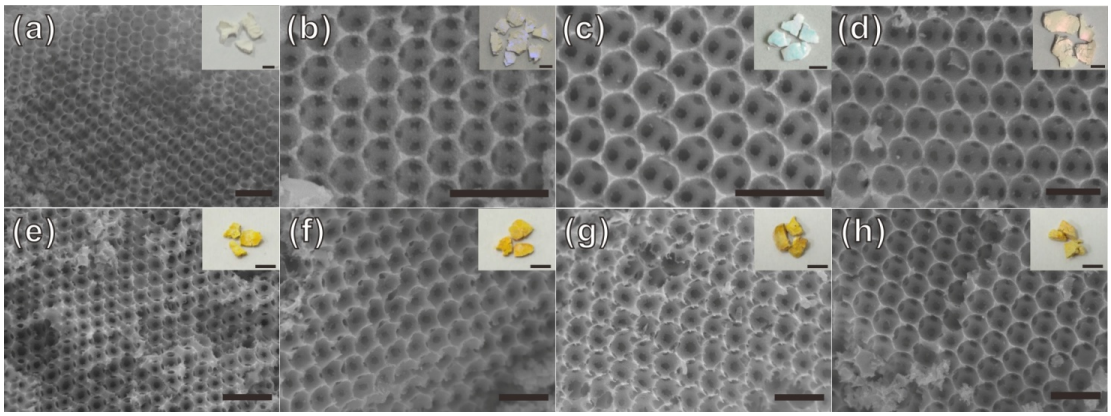

Figure S1. SEM images of (a-d) 3DOM TiO_2 and (e-h) 3DOM TAC with the pore sizes of 160 nm, 200 nm, 250 nm and 340 nm, scale bar = 500 nm. The insets are the corresponding photograph for each sample, scale bar = 5 mm.

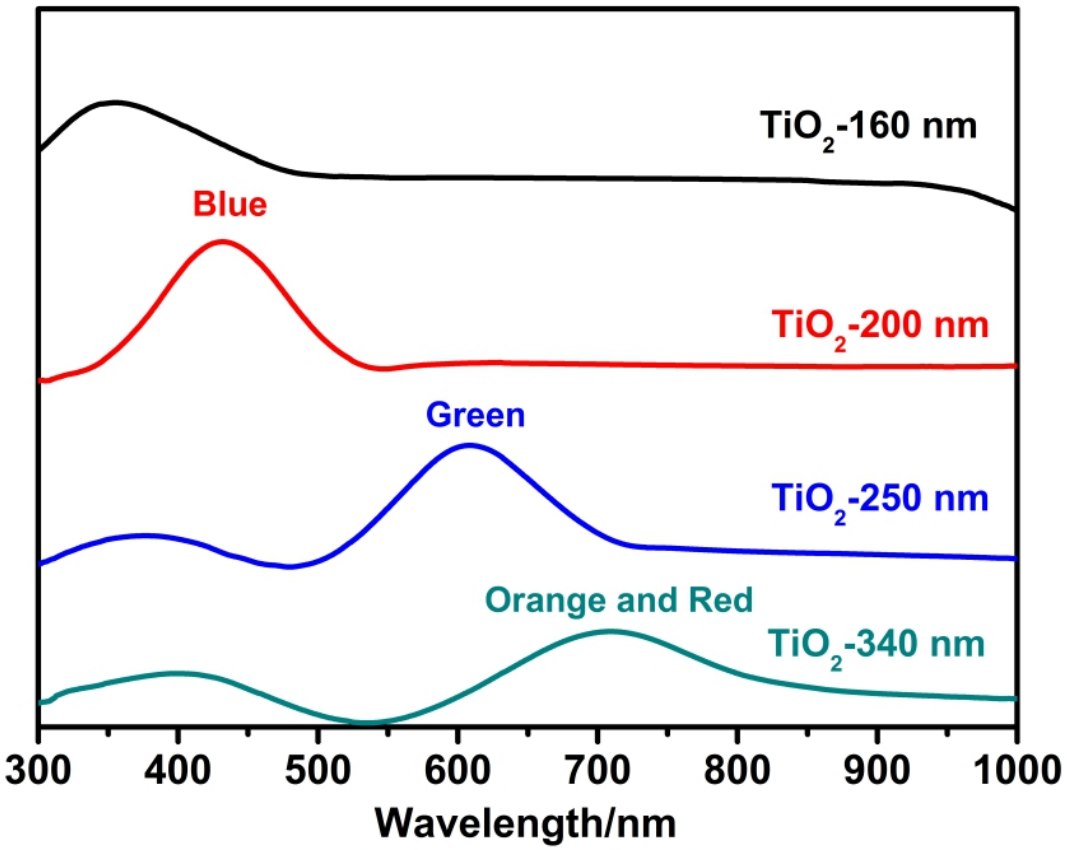

Figure S2. Light reflectance spectra of 3DOM TiO_2 with different pore sizes measured in air.

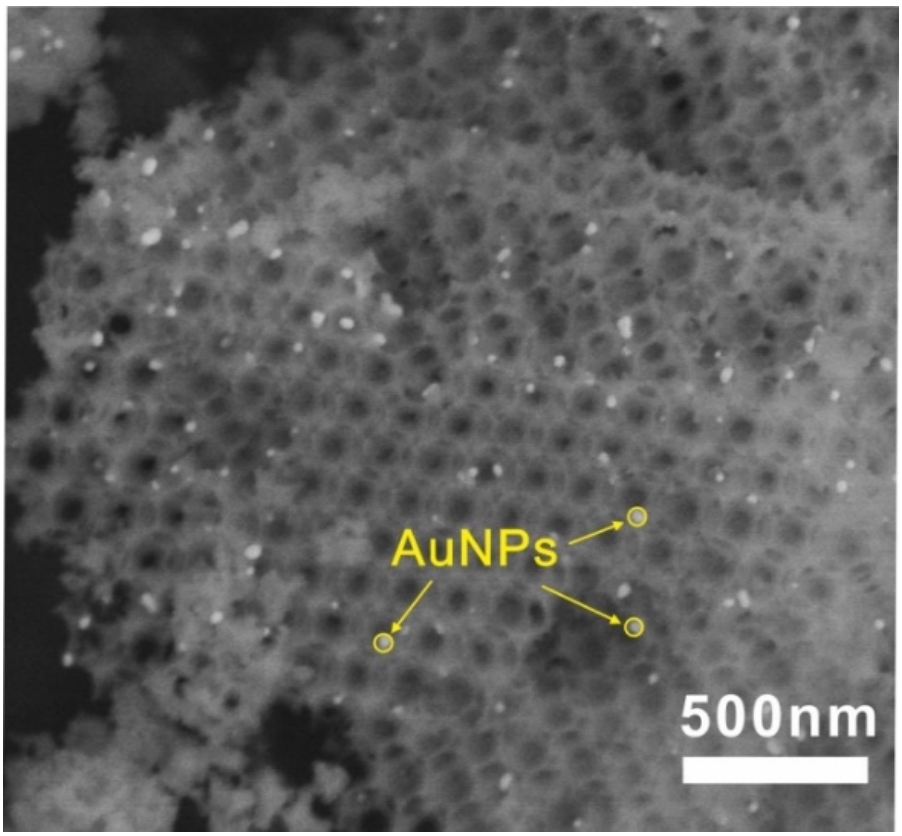

Figure S3. Back scattered electron (BSE) image of 3DOM TAC-250.

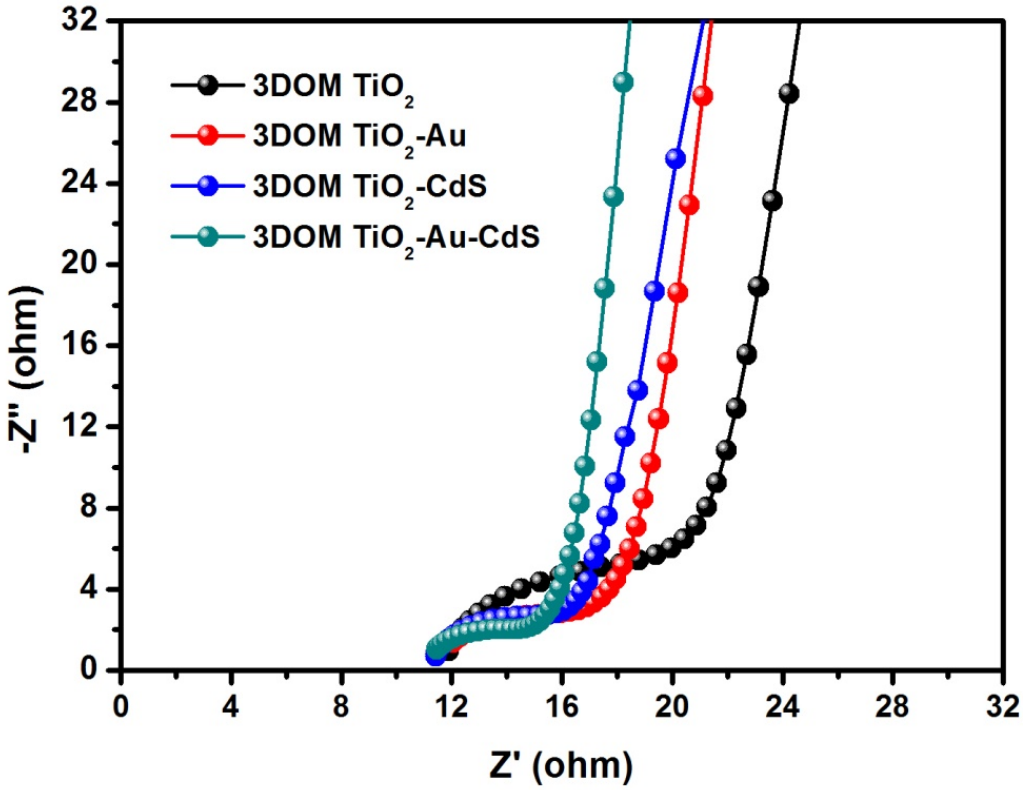

Figure S4. Nyquist plots of 3DOM TiO_2, 3DOM TiO_2-Au, 3DOM TiO_2-CdS and 3DOM TiO_2-Au-CdS in 0.5 M Na_2SO_4 aqueous solution.

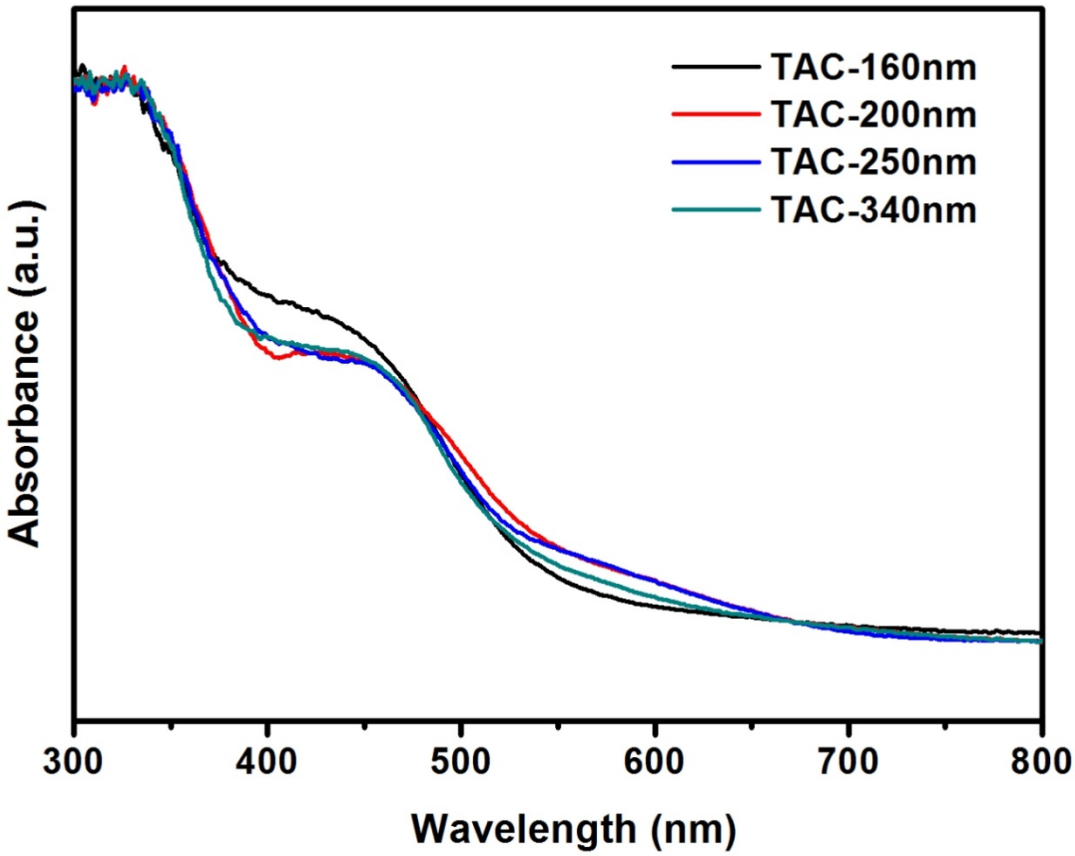

Figure S5. UV-vis absorption spectra of 3DOM TAC with different pore sizes.

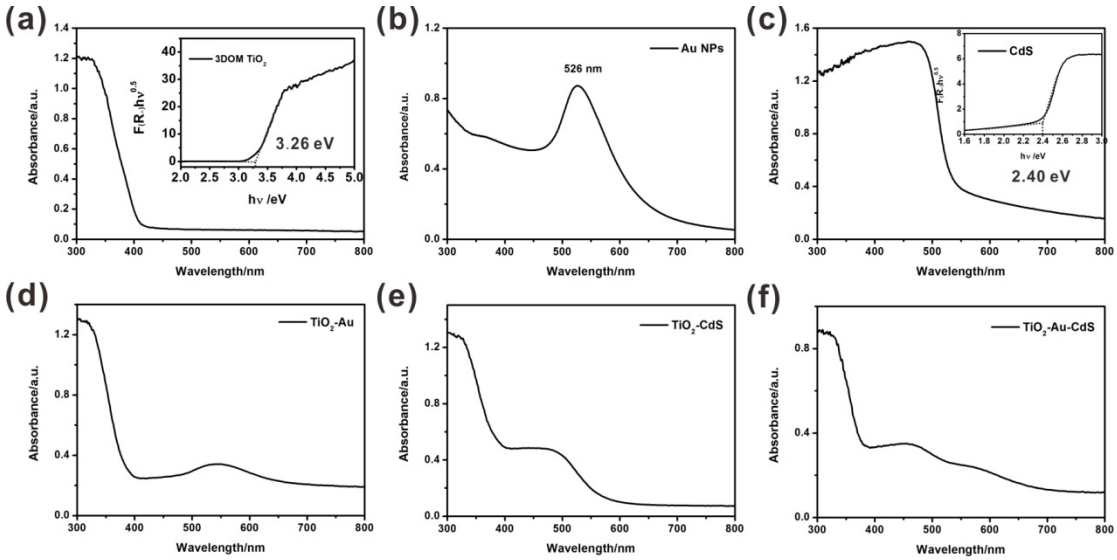

Figure S6. UV-vis absorption spectra of (a) 3DOM TiO_2, (b) Au NPs in solution, (c) CdS, (d) 3DOM TiO_2-Au, (e) 3DOM TiO_2-CdS and (f) 3DOM TiO_2-Au-CdS.

Table S1 The calculated and measured PBG of 3DOM TiO_2 with different pore sizes in water at the incident light angle of 0°.

sample	Macropore size (nm)	First-order reflection		Second-order reflection	
		calculated (nm)	experiment (nm)	calculated (nm)	experiment (nm)
3DOM TAC-160	160	427	417	219	-
3DOM TAC-200	200	533	510	267	-
3DOM TAC-250	250	667	643	334	349
3DOM TAC-340	340	907	800	454	430

Table S2 The calculated H_2 evolution rate for each sample.

Sample	Pore size/nm	H_2 evolution rate/ $mmolh^{-1}g^{-1}$	content of CdS/wt%	H_2 evolution rate by content of CdS/ $mmolh^{-1}g^{-1}$
TAC	-	1.66	18.1	9.17
3DOM TAC-160	160±5	2.55	17.2	14.8
3DOM TAC-200	200±5	1.81	17.1	10.6
3DOM TAC-250	250±5	3.50	16.9	20.7
3DOM TAC-340	340±5	1.96	16.3	12.0
3DOM TAC-380	380±5	2.30	18.2	12.6
3DOM TAC-410	410±5	1.98	16.4	12.1
3DOM TAC-450	450±5	2.59	16.3	15.9

Table S3 Photocatalytic H_2 evolution rate from references.

Photocatalyst	Structure	Incident light/nm	H_2 evolution rate/mmolh^{-1}g^{-1}	Reference
Our sample	3DOM	300W Xe (>420nm)	3.5	-
CdS-TiO_2	3DOM	300W Xe (>420nm)	0.18	[1]
Pt/CdS/Au/$TiO_{1.96}C_{0.04}$	nanoparticle	300W Xe (>420nm)	2.9	[2]
CdS-Au- TiO_2	butterfly wing	750W Xe (full)	0.064	[3]
Au@TiO_2-CdS	nanoparticle	300W Xe (>420nm)	2.0	[4]
CdS/Au/N- TiO_2	leaf-inspired hierarchical porous	750W Xe (>400nm)	0.017	[5]
CdS-Au- TiO_2	Biomass-derived hierarchical porous	750W Xe (full)	0.14	[6]
CdS-Au-WO_3	3DOM	300W Xe (>420nm)	1.6	[7]
CdS/Au/3DOM-$SrTiO_3$	3DOM	300W Xe (>420nm)	2.7	[8]

[1] H. Zhao, M. Wu, J. Liu, Z. Deng, Y. Li, B.-L. Su, Appl. Catal. B-Environ. 184 (2016) 182-190.

[2] H.J. Yun, H. Lee, N.D. Kim, D.M. Lee, S. Yu, J. Yi, ACS Nano 5 (2011) 4084-4090.

[3] L. Ding, H. Zhou, S. Lou, J. Ding, D. Zhang, H.X. Zhu, T.X. Fan, Int. J. Hydrogen. Energ. 38 (2013) 8244-8253.

[4] J. Fang, L. Xu, Z.Y. Zhang, Y.P. Yuan, S.W. Cao, Z. Wang, L.S. Yin, Y.S. Liao, C. Xue, ACS Appl. Mater. Inter. 5 (2013) 8088-8092.

[5] H. Zhou, L. Ding, T.X. Fan, J. Ding, D. Zhang, Q.X. Guo, Appl. Catal. B-Environ. 147 (2014) 221-228.

[6] H. Zhou, J.Y. Pan, L. Ding, Y.W. Tang, J. Ding, Q.X. Guo, T.X. Fan, D. Zhang, Int. J. Hydrogen Energ. 39 (2014) 16293-16301.

[7] X.F. Cui, Y.J. Wang, G.Y. Jiang, Z. Zhao, C.M. Xu, Y.C. Wei, A.J. Duan, J. Liu, J.S. Gao, RSC Adv. 4 (2014) 15689-15694.

[8] Y. Chang, K. Yu, C.X. Zhang, Z.Q. Yang, Y.J. Feng, H. Hao, Y.Z. Jiang, L.L. Lou, W.Z. Zhou, S.X. Liu, Appl. Catal. B-Environ. 215 (2017) 74-84.